Supporting Information

Peptide-Decorated Tunable-Fluorescence Graphene Quantum Dots

Bedanga Sapkota,[1] *Abdelkrim Benabbas,*[1] *Hao-Yu Greg Lin*,[2] *Wentao Liang,*[3] *Paul Champion,*[1] *and Meni Wanunu*[1,‡,*]

[1]Department of Physics, Northeastern University, Boston, Massachusetts 02115

[2]Center for Nanoscale Systems, Harvard University, Cambridge, Massachusetts 02138

[3]Department of Biology, Northeastern University, Boston, Massachusetts 02115

[‡]Department of Chemistry and Chemical Biology, Northeastern University, Boston, Massachusetts 02115

Corresponding Author

*Email: wanunu@neu.edu

1. Experimental Section:

Transfer of GQDs dispersed in methanol to water

A suspension of colloidal GQDs in methanol was first evaporated to dryness using a rotary evaporator or reduced vapor pressure. Then, dimethyl sulfoxide (DMSO) was added to 5-10% of desired final volume. Once the GQDs were dispersed in DMSO, then desired amount of DI water was added to obtain GQDs in water. It is noted that addition of DMSO as an intermediate solvent is crucial before adding water; direct addition of water led to aggregation of GQDs.

Design of pGQDs

In order to prepare compact, highly water soluble, and biocompatible GQDs, we selected three-domain graphite–binding peptides of 8 amino acid residues in length. These peptides contain either phenylalanine or valine-rich adhesive domain that binds to GQD surface and lysine terminal amino acids to expose DNA-binding moieties. Thus, we exchanged the native surfactants of GQDs with these peptides, hence peptide-modified GQDs (pGQDs) were obtained. The resulting pGQDs are highly soluble in water and PBS and retained the characteristics optical properties of original GQD. We studied morphology and size (diameter and thickness) of the pGQDs by AFM, DLS and TEM after negative staining with uranyl acetate. AFM and TEM images revealed change in contrast, slightly disturb in dispersity, and increased in average diameter by ~4 nm without aggregation of GQDs, upon coating with peptide.

Characterization of peptides on graphene flakes

Graphene flakes were obtained via vigorous mechanical exfoliation of an HOPG layer using scotch tape and pressing the resulting flakes onto a 300 nm thermal SiO_2 film on a Si wafer substrate. Any residual adhesive was removed by rinsing with acetone, followed by subsequent rinses of isopropanol and de-ionized water. To oxidize the surfaces of the flakes, the substrates were immersed in a 100°C nitric acid bath for one hour. We reduced the oxidized flakes by immersing the substrates in 1% hydrazine hydrate in water for 10 minutes and again rinsing with isopropanol and de-ionized water. Raman spectroscopy of the resulting flakes showed thicknesses as low as one layer. Peptide concentration used was 0.136 mg/mL (140 μM) (10 μL, 1.36 mg/mL original solution, 90 μL DI water). The peptide was deposited *in-situ* while imaging

using ~200μL of imaging buffer. All resulting samples were imaged in liquid with AFM (Dimension Icon, FastScan-type scan head) using a soft, sharp (k = 0.4 N/m, nominal tip radius = 5nm) cantilever in Peak-Force imaging mode. While imaging the biological samples, peak force setpoints were kept below 4 nN.

Measuring persistence length

To find the DNA persistence length from the AFM images, each DNA molecule was traced, quantified and analyzed using NCTracer software, developed by Neurogeometry lab at Northeastern University (http://www.northeastern.edu/neurogeometry/resources/tools/). In order to find the persistence length l_p of the DNA in the absence and presence of pGQDs, local bend angle θ for different locations along the DNA were measured as a function of DNA contour segment length L, and fitted to a two-dimensional WLC model as shown below:

$$<(\cos(\theta)>=e^{-L/2lp} \quad (1)$$

Dynamic light scattering

For DLS measurement, a solution of DNA-pGQD complex was prepared by pre-incubating a colloidal solution of pGQDs (200 μL, 0.51 μM) in water with DNA (1 mL, 4.2 nM) at room temperature for 5 h.

Cell imaging

Michigan cancer foundation (MCF-10A) epithelial cells were cultured in DMEM media (Dulbecco's modified Eagle's medium supplemented with 10% fetal bovine serum and 1% penicillin/streptomycin) using a four-chambered Lab-Tek coverglass system (Thermo Scientific Nunc Lab-Tek). All cells were incubated at 37 °C in 5% CO_2 incubator until approximately 80-90% confluence was reached. Different concentration of pGQDs (3.0 and 4.5 μM) in culture media were added to two wells of glass slide chambered and third well was used as a control in which epithelial cells were grown. After incubation at 37 ^{0}C for 6 h, the extracellular remaining of GQDs were removed by washing with 1×DPBS (Dulbecco's phosphate buffered saline) solution and then fresh serum free media was added. After incubation at 37 ^{0}C for another 10

min, cells were directly imaged on a Zeiss LSM 700 confocal microscope system with excitation wavelength of 405 nm.

2. Supplementary Figures

Atomic force microscopy images and thickness distributions of a series of hydrazine treated graphene quantum dots dispersed in water:

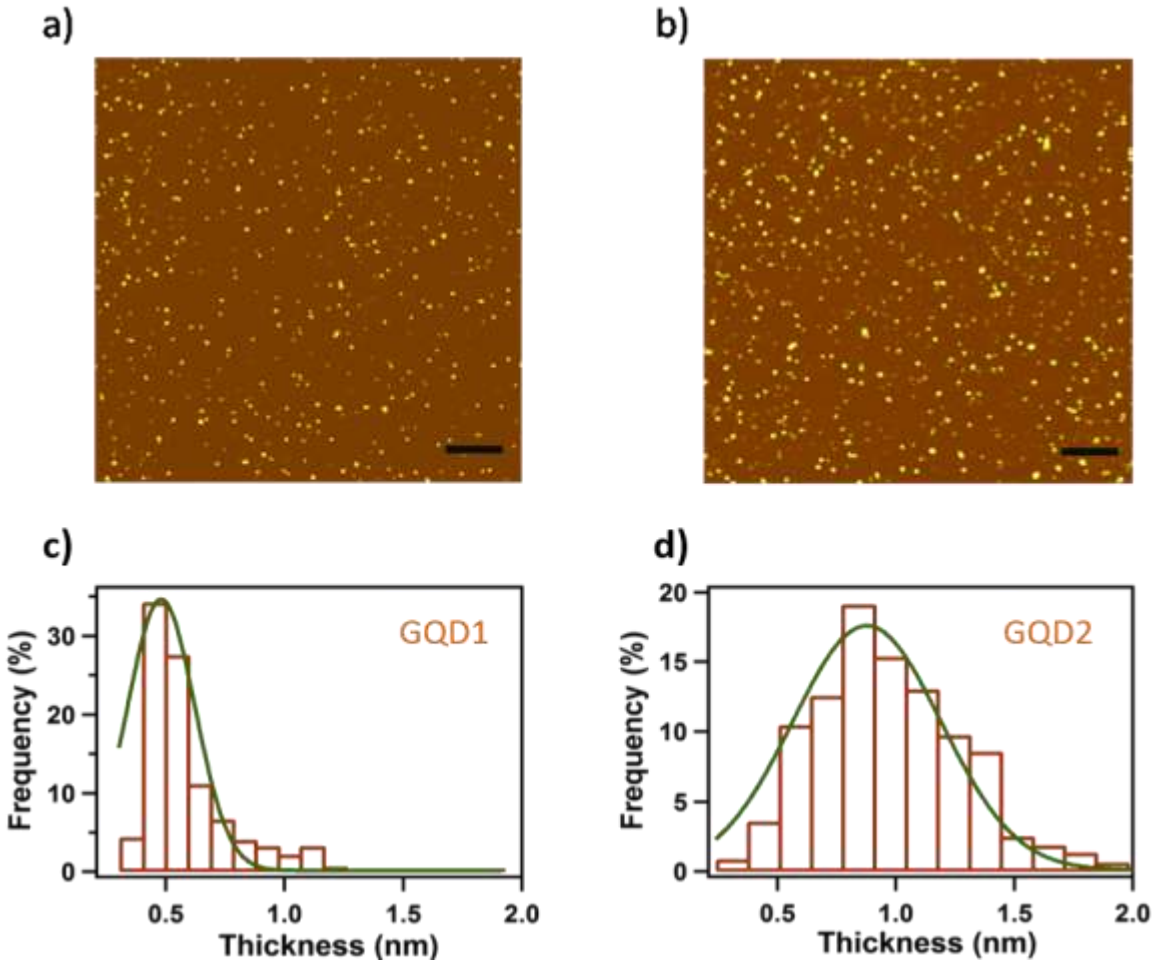

Figure S1: Analysis of hydrazine-treated graphene quantum dots. (a) AFM topography of GQD1. (b) AFM topography of GQD2. (c) Thickness distribution of GQDs shown in image a, showing monolayer nature of GQD1. (d) Thickness distribution of GQDs shown in image b, average thickness of GQD2 is 0.89 nm (bilayer) with S.D. 0.16. (Scale bar: 200 nm)

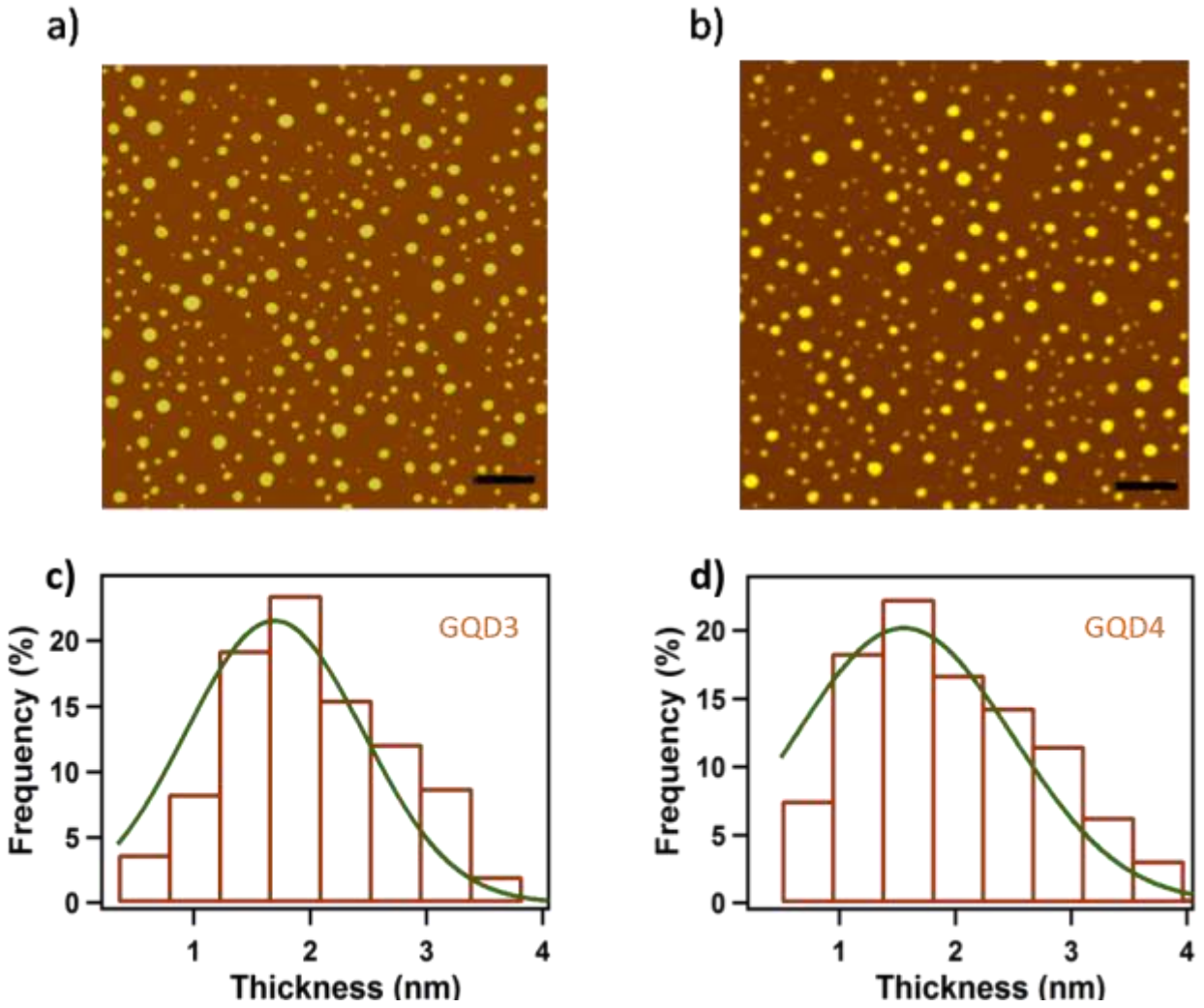

Figure S2: Analysis of hydrazine-treated graphene quantum dots. (a) AFM micrograph of GQD3. (b) AFM micrograph of GQD4. (c) Thickness distribution (histogram) of GQDs shown in image a, showing average thickness of 1.54 nm with S.D. 0.45 nm. (d) Diameter distribution of GQDs shown in image b, showing average thickness of 1.69 nm with S.D. 0.68 nm. (Scale bar: 200 nm)

Transmission electron microscopy images of a series of the GQDs dispersed in water:

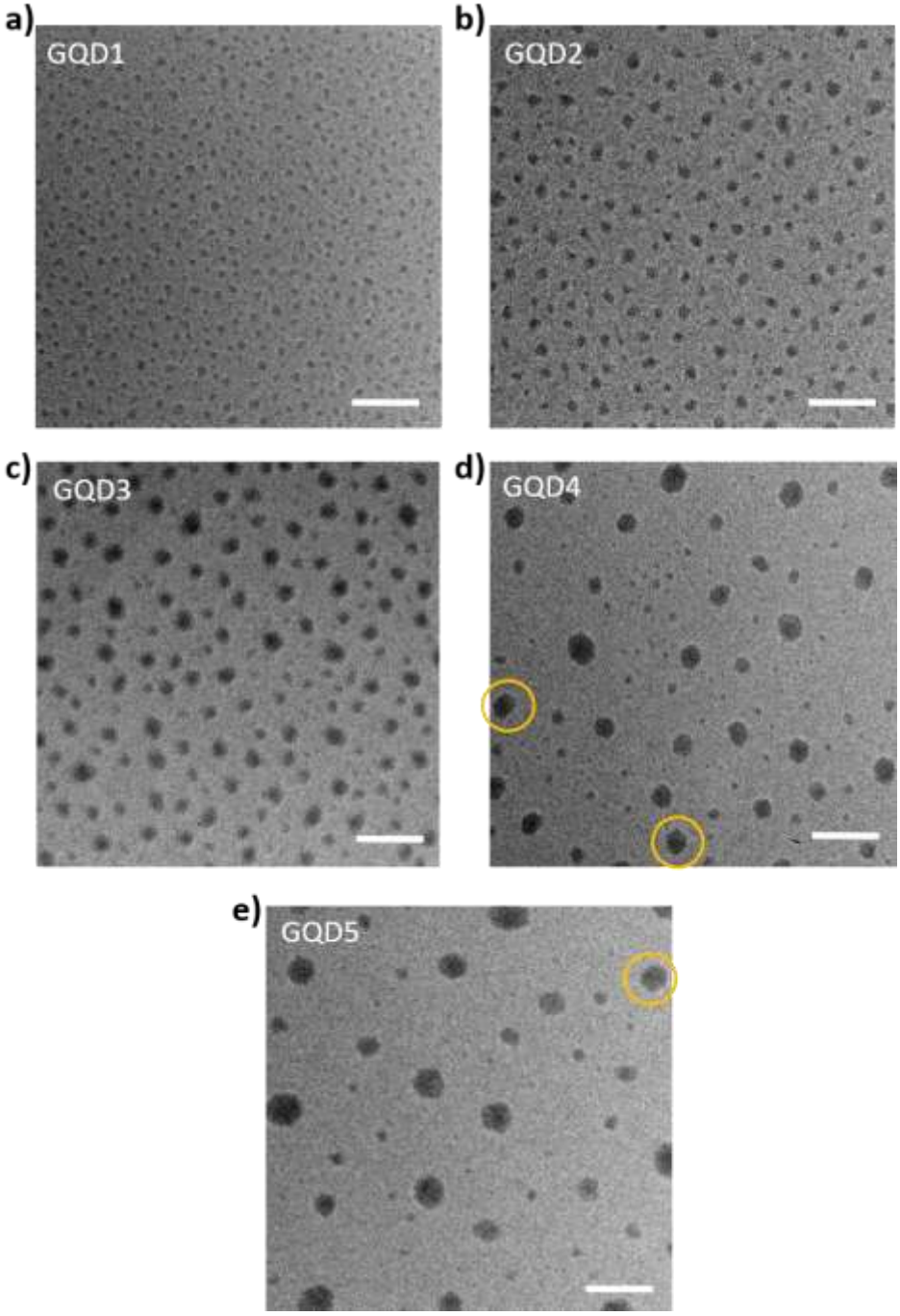

Figure S3: Bright field TEM images of a series of chemically reduced GQDs (all scale bars 100 nm). Smaller GQDs (GQD1, GQD2, and GQD3) are thinner and sheet or flake like structure (a-c, ~~b~~) whereas bigger (d, e) are more or less hexagonal structure (yellow circles).

Fluorescence properties of a series of the GQDs:

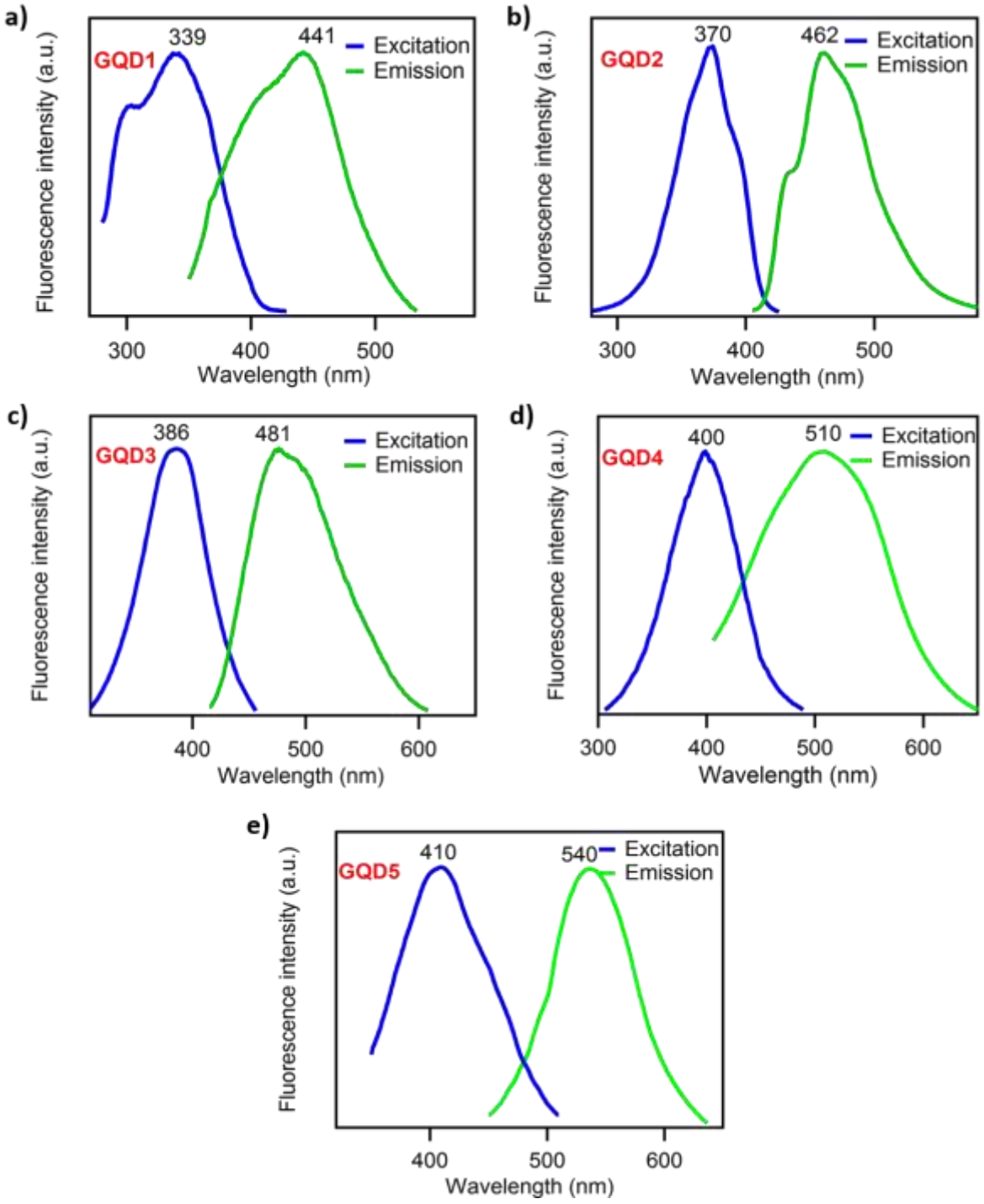

Figure S4: PL spectra of a series of the GQDs shown in Figure 1b (see main paper). (a-e) Excitation (blue line) and emission (green line) spectra of GQD1, GQD2, GQD3, GQD4, and GQD5. Average particle diameter is shown in **Figure** 1c.

Emission quantum yield (QY) measurement

The emission QY of the GQDs was determined using riboflavin as a reference. Excitation wavelength, slit width, and PMT voltage were kept constant and the QY was calculated using following equation:

$$QY = QY_R\,(I/I_R)\,(A_R/A)\,(\eta/\eta_R)^2 \qquad (2)$$

Where the subscript "R" refers to the reference, I is the integrated fluorescence intensity, A is the absorbance at the wavelength of excitation (355 nm), and η is the refractive index of the solvent (water in both measurements). Quantum yield of riboflavin excited at 355 nm (QY_R) =0.39,[1] A=0.25, A_R=0.06, and $\eta = \eta_R$ for the same solvent. With all these values, quantum yield of GQDs is found to be 0.64. Emission spectra for both reference and GQD sample are shown below.

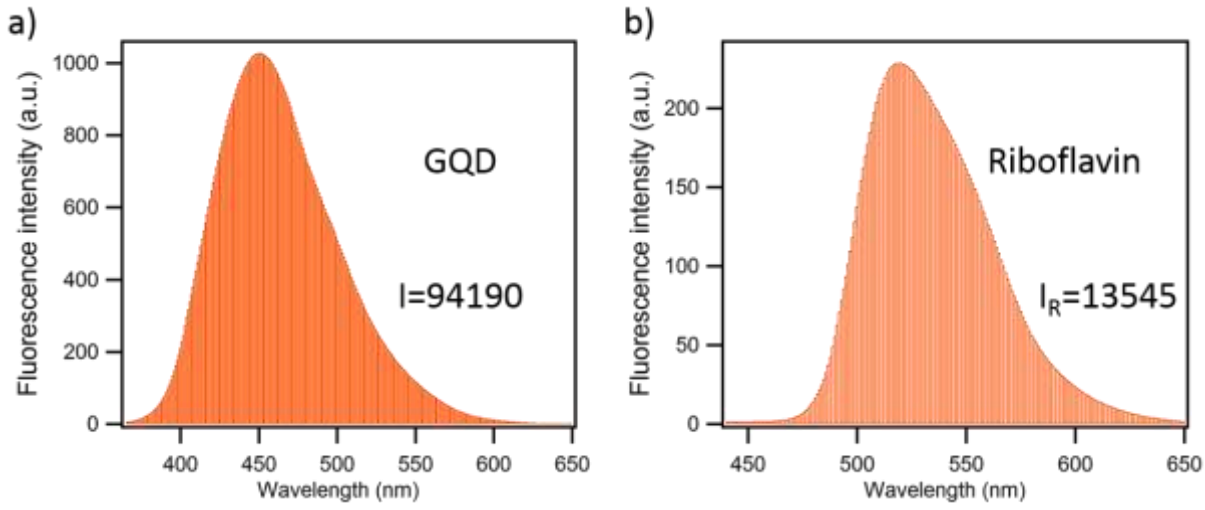

Figure S5: (a) Emission spectra of GQD excited at 355 nm. (b) Emission spectra of riboflavin (reference) excited at 355 nm.

Measuring two-photon absorption (TPA) cross section

TPA cross-section of GQDs was measured using riboflavin as a reference and based on the equation shown below:

$$\sigma = \sigma_{ref} \ (F/F_{ref}) \ (\Phi_{ref}/\Phi) \ (C_{ref}/C) \qquad (3)$$

Where subscript "ref" refers to the reference compound riboflavin, F is the integral fluorescence intensity, Φ stand for the quantum yield, and C is the concentration.[2] TPA cross section of riboflavin with excitation at 800 nm can be obtained from the literature.[1]

Table S1: Control parameters of synthesis process with average diameter of a series of the graphene quantum dots shown in **Figure** S3 and S4.

Nano-crystal	Average diameter (nm)	OA (Vol.%)	Octadecene (mL)	Oleylamine (mL)	Total volume (mL)
GQD1	14±4.1	40	12	8	20
GQD2	19±2.9	30	14	6	20
GQD3	26±3.6	20	16	4	20
GQD4	30±6.7	10	18	2	20
GQD5	34±6.9	5	19	1	20

IR spectra of a series of the GQDs:

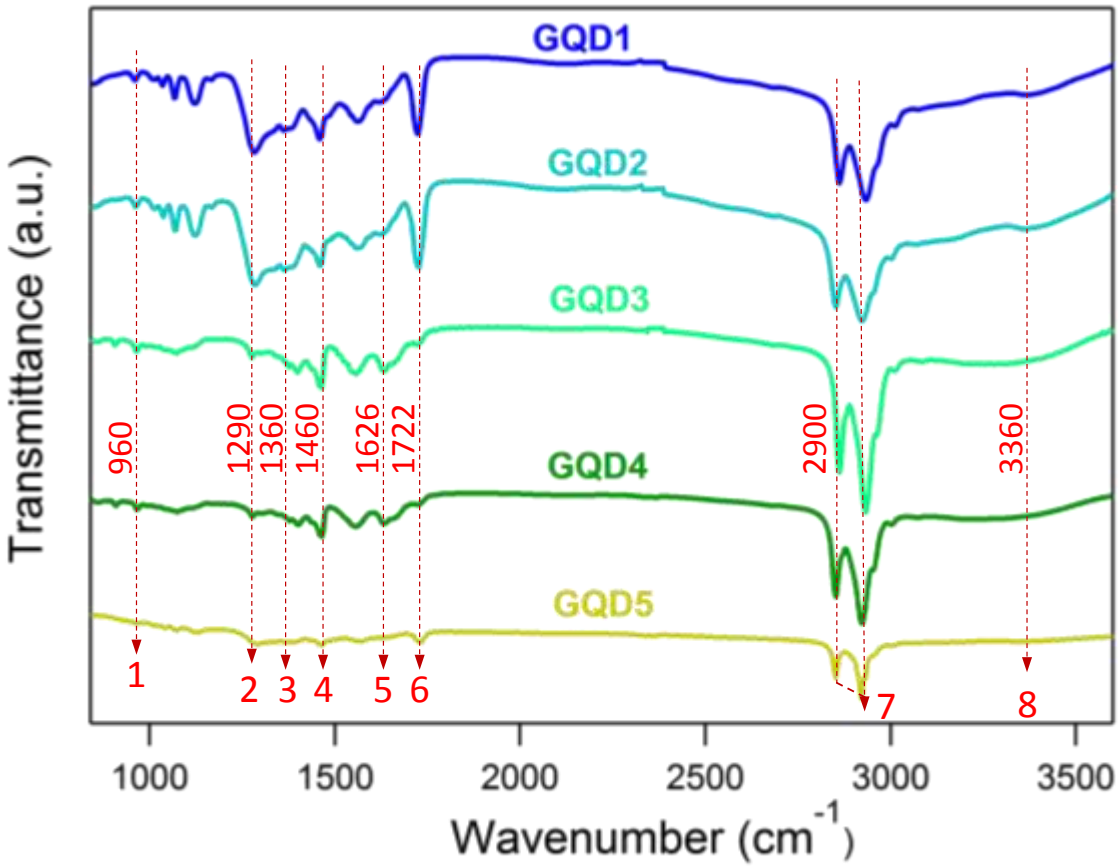

Figure S6: IR spectra of a series of the GQDs shown in **Figure** S4.

Peak 1 is assigned to the alkenyl group of oleylamine. Peak 2 is attributed to the C-O stretching of carboxylic groups on the GQDs. Peak 3 and peak 4 are assigned to the C-N stretching and the amide N-H bending, respectively.[3] Peak 5, peak 6 are assigned to the stretching vibration of C=C and C=O in carbonyl groups.[4] Peaks in 7 (stretching vibration C-H) and peak 8 (stretching vibration N-H) are assigned to alkyl group and amine group of oleylamine, respectively.

Fluorescence property of GQDs at different pH:

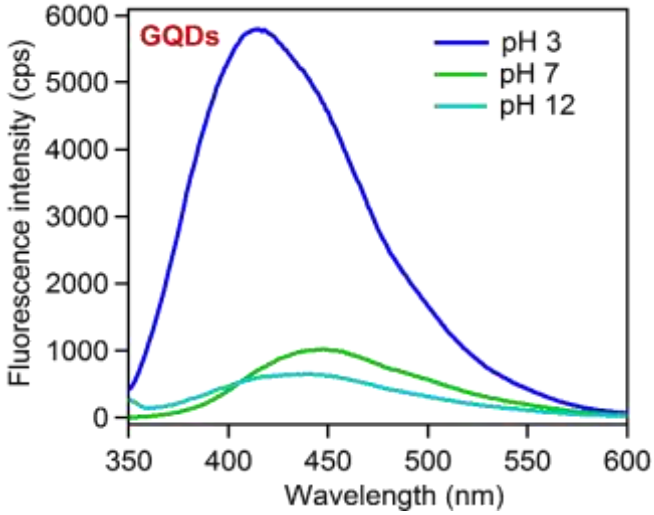

Figure S7: pH-dependent fluorescence spectra of GQDs dispersed in water. Each sample was centrifuged at 5,000 rpm for 5 min after adding acid (HCl) or base (KOH) and pH was measured using pH meter. Note that concentration of each of the sample was kept constant by adding equal volume of either acid or base or water to the original GQDs dispersion in water.

To gain a better understanding of the dependence of PL on the chemical environment of GQDs, the changes in PL property on varying pH value were studied. Interestingly, the PL of GQDs has also been found sensitive to pH (see **Figure** S7). Unlike to earlier reported GQDs where red shift is reported while changing pH from 6 to 3,[5] slight blue shift by 15 nm with decreasing intensity was observed as the pH changed from 7 to 3. In contrary, small red shift by 13 nm with decreasing intensity was observed as the pH changed from 7 to 12 (data not shown). In the same acidic environment, blue shifted by 39 nm (from 448 to 409 nm) with significant increasing intensity of GQDs by factor of 5 was observed upon centrifugation at 5000 rpm for 5 min (**Figure** S7, blue line). While in alkaline solution, no effect was observed under the same condition. This could be due to rapidity in ozonation mechanism (responsible for increasing intensity) and chain decomposition i.e. breaking of carbon-carbon bonds from the basal plane[6]

(for blue shift) in acidic environment of GQDs upon centrifugation. Acid-evoked fluorescence enhancement is also reported with carbon dots in strong acidic environment[7] and intramolecular charge transfer is purposed for the mechanism of such enhancement.[8] Furthermore, in the acid-base aqueous solution, there are two forms of ozone namely dissolved ozone and $HO^{\cdot}$ radical.[9] Yong et al. reported that the dissolved ozone directly reacted with GQDs in acidic environment based on high-resolution C1s XPS spectra measurement of GQDs.[6] The ozonation reaction formed oxygen-containing functional group and the fluorescence intensity increases with the increase in oxygenated species.[10-11]

Hydrodynamic diameter distribution of GQDs and peptide:

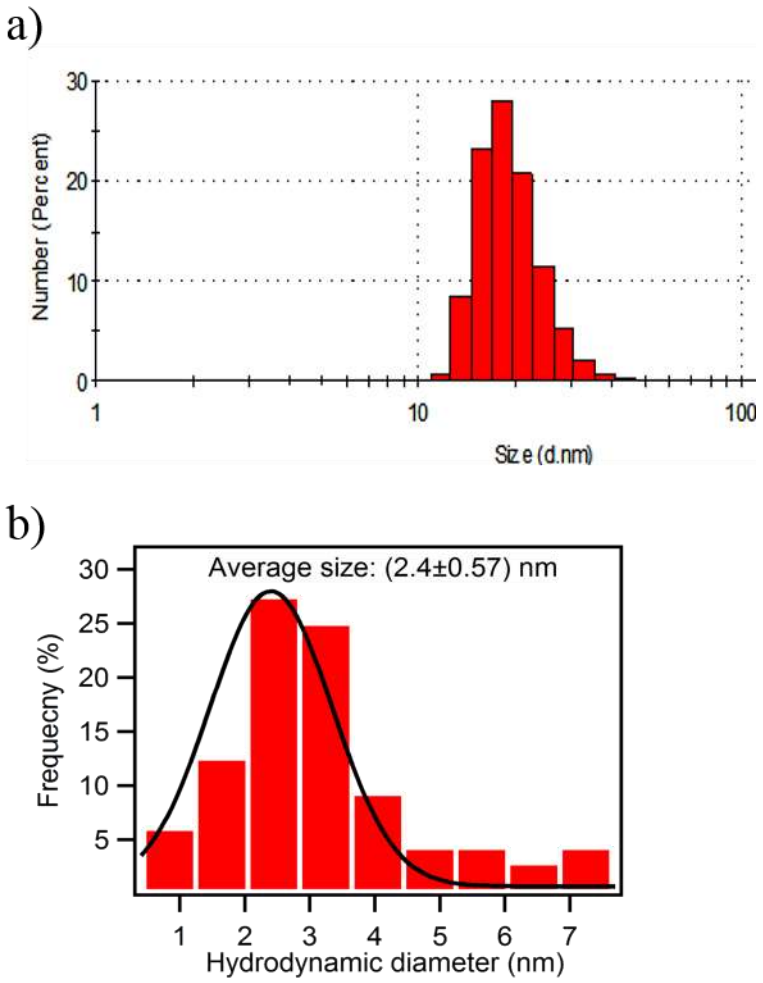

Figure S8: (a) Hydrodynamic diameter distribution of GQD2 (3.3 µM**)** from Dynamic light scattering (DLS)**.** (b) Hydrodynamic diameter distribution of peptide (4.13 µM**)** from DLS.

Figure S9: Stability of peptide-modified GQDs (pGQDs) over time.

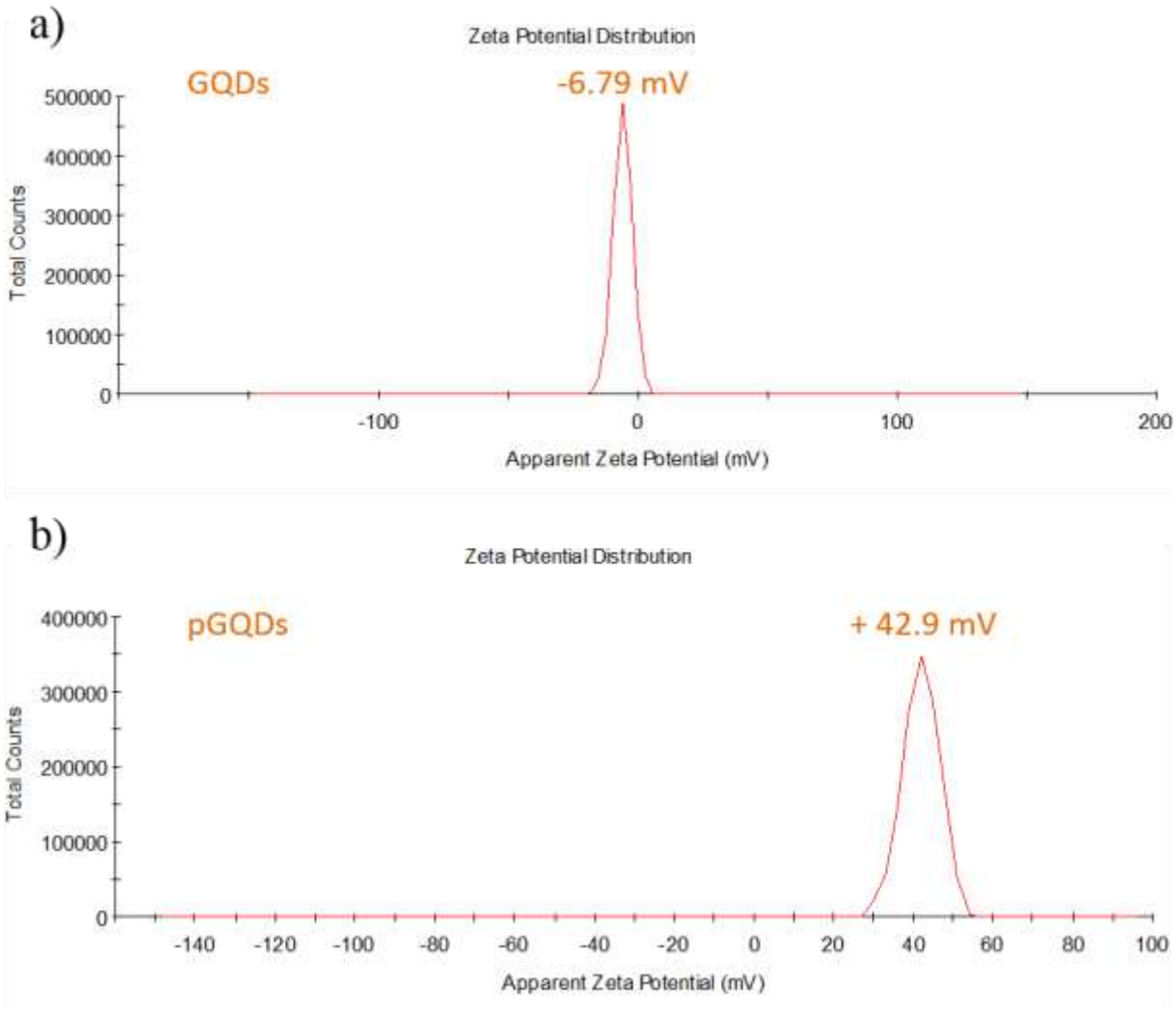

Figure S10: The zeta potential of GQDs (a) and peptide-modified GQDs (b) in water.

Characterization of GQDs and peptide-modified GQDs (pGQDs):

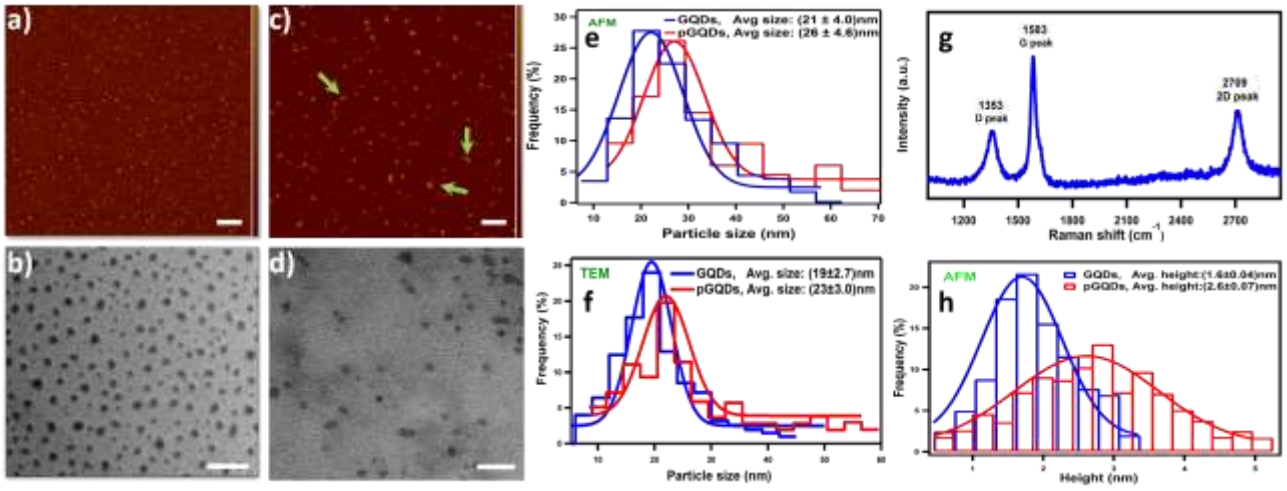

Figure S11: Characterization of GQDs before and after peptide-functionalization. (a and c) AFM images of GQDs before (a) and after functionalization with peptide (c). (b and d) TEM images before (b) and after modification (d). Change in contrast of dots are due to difference in the number of layers. Dispersity of GQDs slightly disturbed by the addition of peptide. Peptide bridges GQDs (arrows). (Scale bars: 200 nm). (e and f) Diameter distribution of GQDs and pGQDs from AFM (e) and TEM (f). (g) Raman spectrum of GQDs shows high quality graphene (I_D/I_G=0.74 and I_G/I_{2D}=1.23) and graphene peak at 1583 cm^{-1}; was obtained by casting highly concentrated GQDs on Si/SiO_2 substrate and using Ranishaw Ramascope with 488 nm laser as an excitation source. (h) Height distribution shows average height increased by ~ 1 nm after modification.

Raman spectroscopy:

Raman spectroscopy was performed using Renishaw Ramascope with the laser (488 nm) as excitation source. The laser power at sample was below 1 mW to avoid laser induced heating and SiO_2 (300 nm)/Si wafer was used as a substrate.

Figure S12a compares the Raman spectra of pristine, oxidized and chemically reduced graphene recorded from the same graphene flake after each treatment process. The intensity ratio of D and G band (I_D/I_G) for the pristine, oxidized and chemically reduced graphene is 0.20, 0.38,

and 0.27 respectively. The increase in intensity ratio (from 0.20 to 0.38), indicating that oxidation process introduce a significant distortion of the aromatic rings and decrease in ratio (from 0.38 to 0.27) with the hydrazine hydrate treatment, indicating that distortion of the 6-fold rings is recovered and the carbon lattice returns to an essential graphitic state.[12] The 2D band of the oxidized graphene shows decrease in relative intensity compared to the G band, an effect that has been related to the presence of defects in graphitic materials.[13]

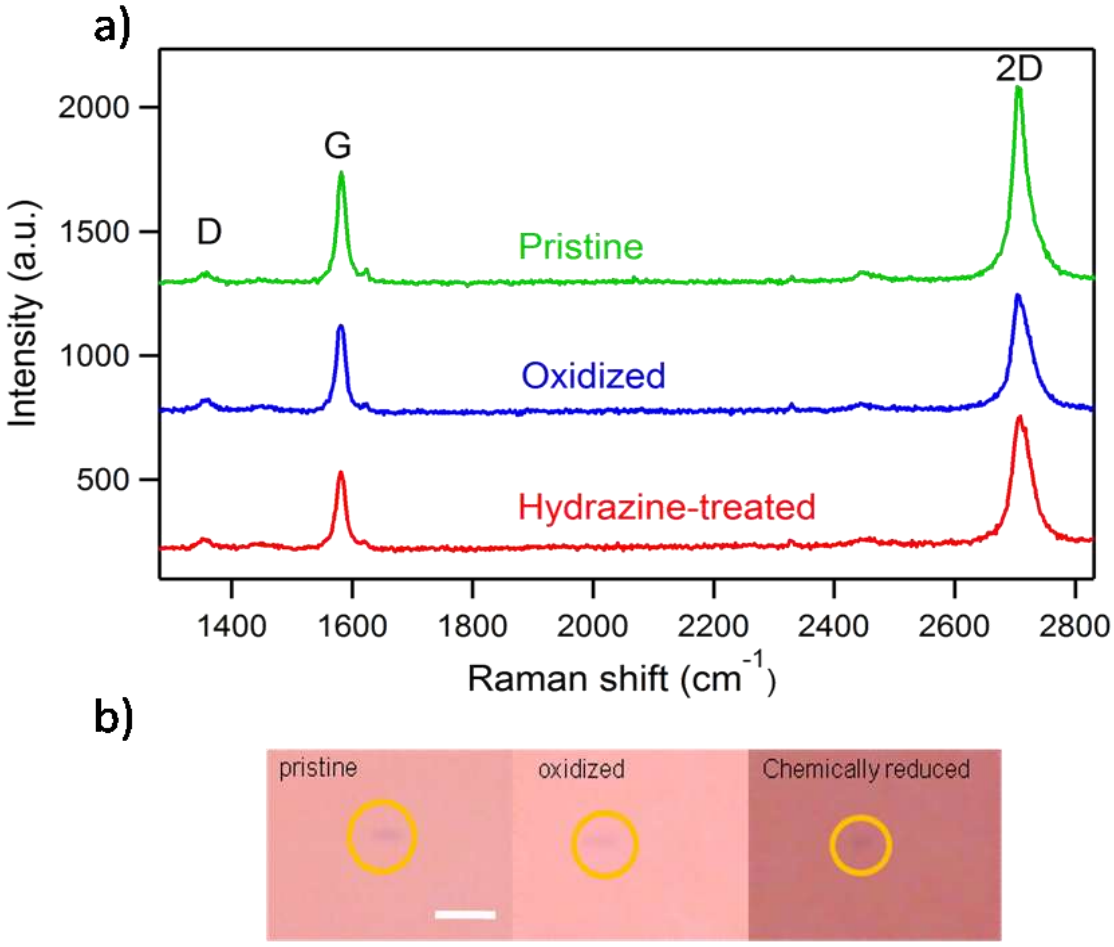

Figure S12: a) Raman spectra and optical images of graphene flakes. "Pristine" graphene: exfoliated from graphite. "Oxidized" graphene: immersed in hot 100°C nitric acid for 1 hour to lightly oxidize. "Hydrazine-treated": Immersed in 1% Hydrazine Hydrate in de-ionized water for 10 minutes following oxidization. 2D band of Hydrazine-treated graphene is slightly blue shifted by ~5nm compare to pristine and oxidized graphene. b) Optical images of pristine, oxidized, and chemically reduced graphene flakes on SiO_2 (300 nm)/Si substrate. For comparison purpose,

Raman spectra shown in **Figure** S12a were recorded from the same flake after each treatment process. Scale bar: 1 μm.

TEM micrograph showing absence of binding of GQDs to DNA:

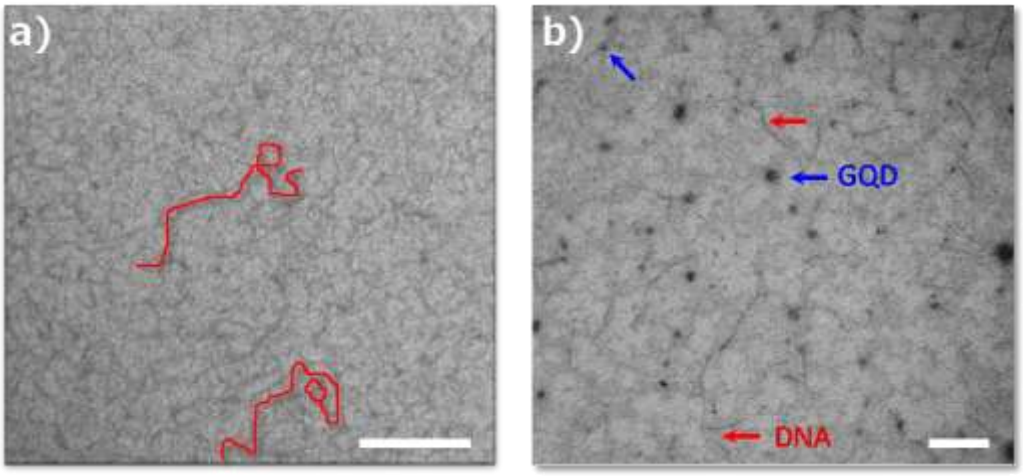

Figure S13: Unmodified GQDs do not specifically bind to DNA. TEM images of (a) DNA (2,000 bp) and (b) DNA-GQDs complex. Two DNA molecules are traced in Figure (a) to aid visualization. Arrow heads show individual GQD and DNA molecule that do not bind to each other. (Scale bars: 200 nm). Because of the low contrast of the DNA biomolecule under TEM, reader is referred to web version of this article.

Binding mechanism and correlation plot studies of overnight incubated in liquid versus incubated on substrate of pGQDs-DNA complex:

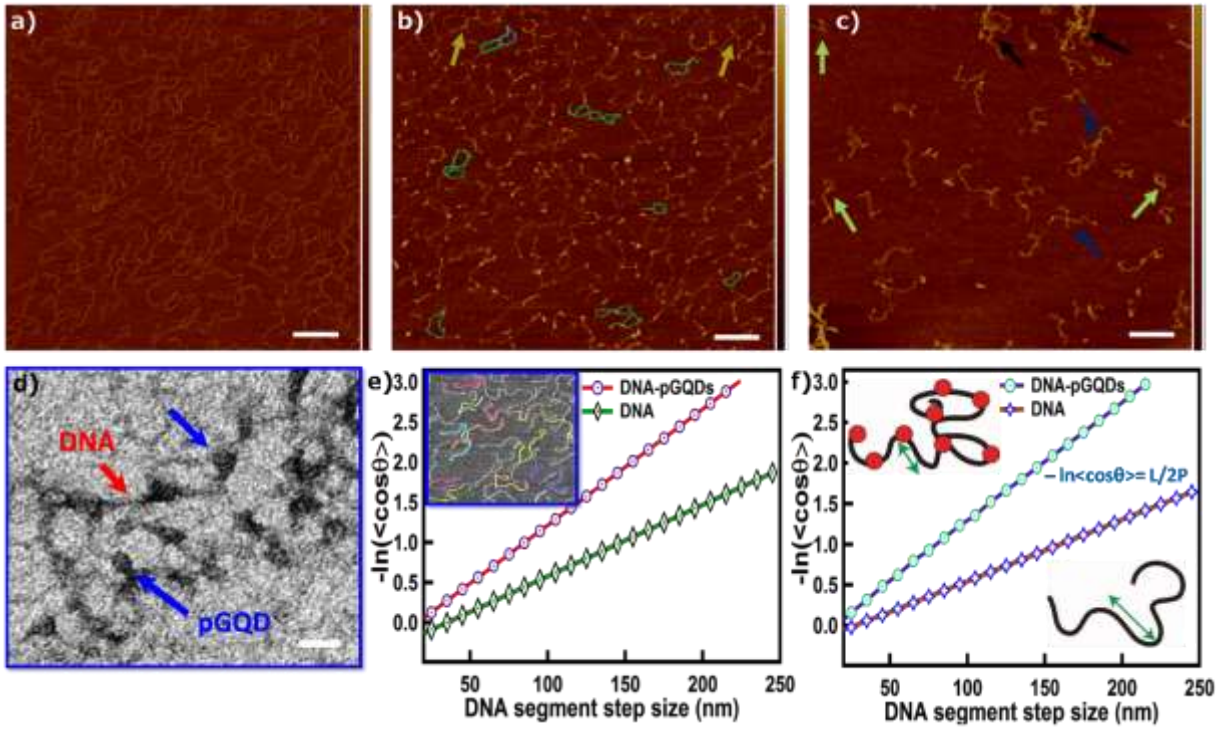

Figure S14: Binding mechanism of pGQDs and DNA, incubated on substrate (mica) versus overnight incubated in liquid (vial). (a) Representative AFM images of DNA (a) and DNA-pGQDs complex incubated on a mica surface for 30 min (b) and overnight incubated in liquid (c). Arrows (image b) show pGQDs that are binding and subsequently bridging DNA molecules and thus promoted DNA networks and loops. Under sufficient binding condition (image c) in liquid, pGQD promoted intramolecular (green), intermolecular (blue), and multimolecular (black) DNA bridges. (Scale bars (a, b, c): 400 nm). (d) TEM image of a uranyl acetate stained DNA-pGQD complex (scale bar: 30 nm). (e and f) Correlation plot shows persistence length of DNA-pGQDs incubated in liquid (f, purple line, 29 ± 6 nm) is slightly less than incubated on mica surface (e, red line, 35 ± 5 nm) from a 2D WLC model . Inset (e) shows automated tracing of DNA molecules from AFM image using NCTracer software.

It is crucial to microscopically examine the single DNA-pGQDs complex in order to probe binding/interaction mechanism. High-quality AFM imaging enable us to clear observation of each bound pGQD position on single DNA molecule. So, we quantitatively examine large number of individual molecules of overnight incubated complex in liquid (for sufficient binding) and found that pGQD promotes three distinct types of bridging. Consistent with this notion, a representative image shown in **Figure S14c** reveals that coexistence of intramolecular (green arrows), intermolecular (blue arrows) and multimolecular (black arrows) DNA bridges promoted by pGQDs, thus implying that pGQD has ability to fold DNA in compact form.

TEM micrograph showing ubiquitous binding of pGQDs to DNA:

Strong contrast of the dots (purple arrows), observed in the micrographs are pGQDs, which are binding and consequently bridging skinny threads like structure DNA (green arrows). In order to aid visualization, DNA molecules are traced out with orange color.

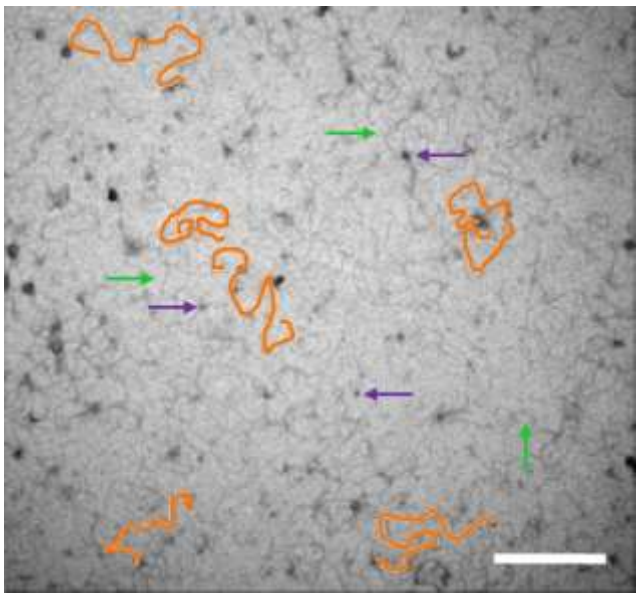

Figure S15: peptide-modified GQDs interact with the DNA molecule. TEM micrograph of the DNA-pGQDs complex. For TEM, DNA was stained with Uranyl acetate (1%). Dark blobs shown by purple arrows are pGQDs that are binding and consequently bridging DNA molecules and formation of loops, networks and compaction of DNA. (Scale bars: 200 nm).

Diameter distributions (histograms) of pGQDs and DNA-pGQDs from dynamic light scattering:

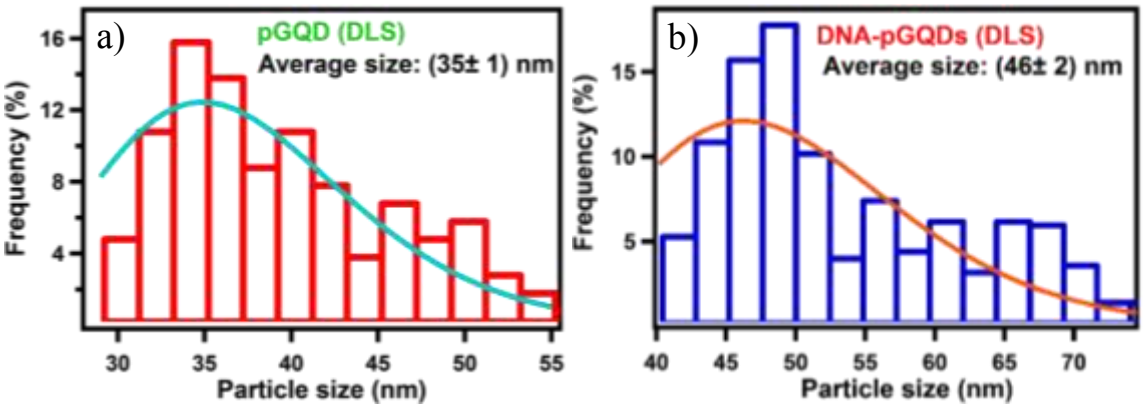

Figure S16: Hydrodynamic diameter distribution of pGQDs (a) and DNA-pGQDs (b) obtained from DLS measurements. Curves are log-normal size distribution fits.

Optical and fluorescence properties:

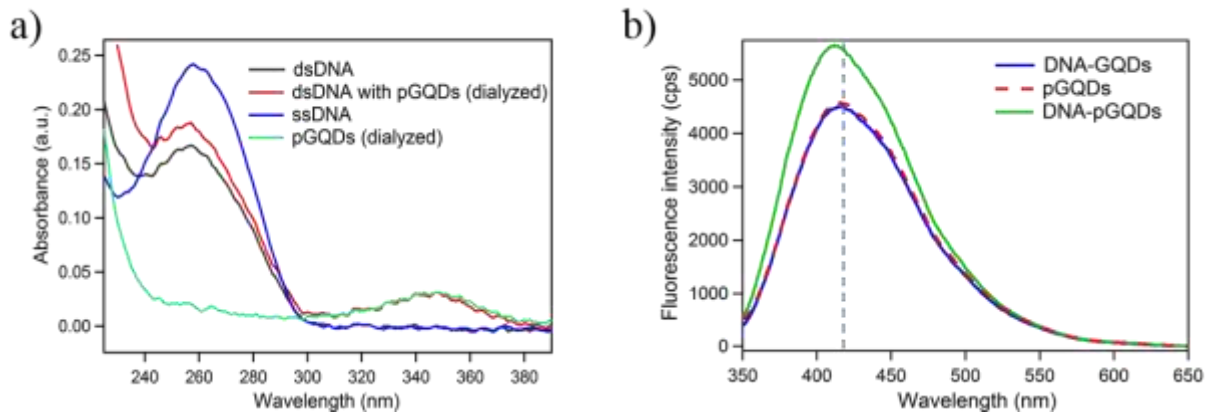

Figure S17: (a) UV-vis spectra of ssDNA, dsDNA, pGQDs, dsDNA-pGQDs. Absorbance of double stranded is 40 % smaller than ssDNA in the region of 260 nm. Absorbance peak of GQDs is clearly observed at ~350 nm with the pGQDs and DNA-pGQDs samples. (b) Fluorescence emission spectra of pGQDs, DNA-GQDs and DNA-pGQDs. Spectrum of GQDs broadens and blue shifts by 8 nm upon DNA binding to pGQDs, while not changing when DNA is incubated with GQDs.

Compact DNA conformations observed with different sizes of pGQD:

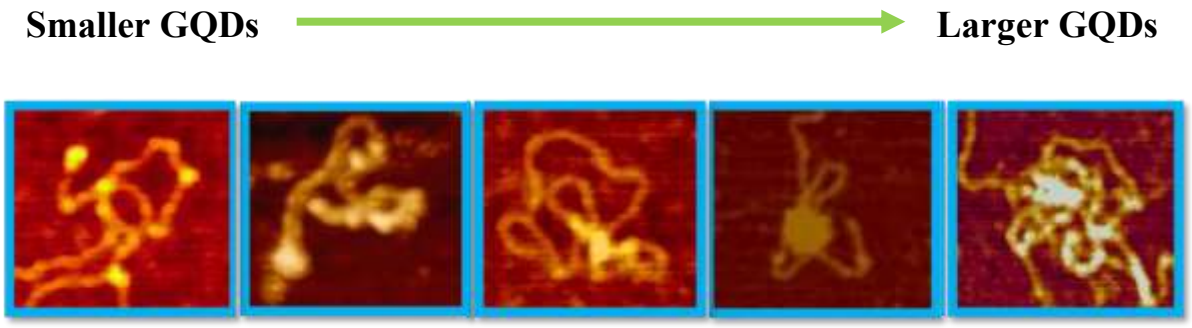

Figure S18: Various examples of 2,000 bp DNA compactization induced by pGQDs

Figure S18 shows DNA wrapping around smaller as well as bigger sizes (diameters) pGQDs under certain control condition (high concentration and long incubation time), such a DNA compaction occurs through a wrapping mechanism could be similar to natural nucleosome

assembly. In addition, controlled DNA condensation itself has many potential applications in medicine and biotechnology.[14]

Two-photon-excited power dependence of PL intensity:

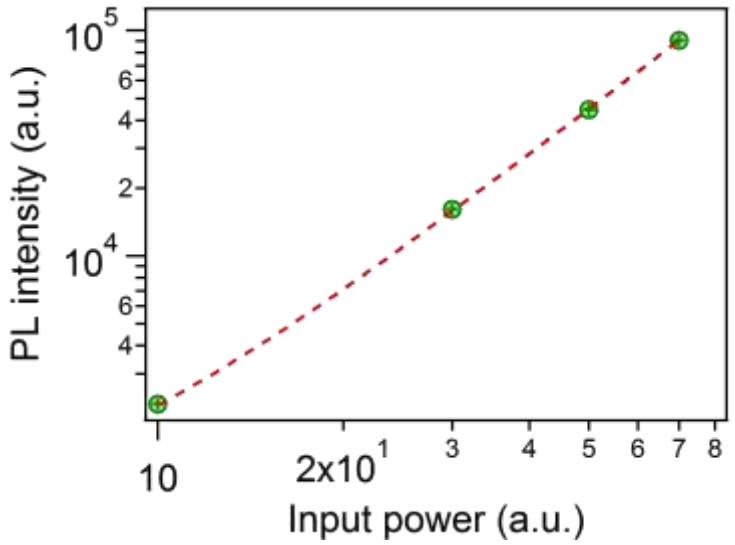

Figure S19: Log-log plot of power dependence of PL intensity. The slope of power depedence is 2.06, which is characteristics of two-photon-excited PL.

References:

1. Bi, Y.-H.; Huang, Z.-L.; Liu, B.; Zou, Q.-J.; Yu, J.-H.; Zhao, Y.-D.; Luo, Q.-M. Two-Photon-Excited Fluorescence and Two-Photon Spectrofluoroelectrochemistry of Riboflavin. *Electrochem. Commun.* **2006,** *8*, 595-599.
2. Pu, S. C.; Yang, M. J.; Hsu, C. C.; Lai, C. W.; Hsieh, C. C.; Lin, S. H.; Cheng, Y. M.; Chou, P. T. The Empirical Correlation between Size and Two-Photon Absorption Cross Section of Cdse and Cdte Quantum Dots. *Small* **2006,** *2*, 1308-1313.
3. Sekiya, R.; Uemura, Y.; Murakami, H.; Haino, T. White-Light-Emitting Edge-Functionalized Graphene Quantum Dots. *Angew. Chem. Int. Ed.* **2014,** *53*, 5619-5623.
4. Liu, Q.; Guo, B.; Rao, Z.; Zhang, B.; Gong, J. R. Strong Two-Photon-Induced Fluorescence from Photostable, Biocompatible Nitrogen-Doped Graphene Quantum Dots for Cellular and Deep-Tissue Imaging. *Nano Lett.* **2013,** *13*, 2436-2441.
5. Ye, R.; Xiang, C.; Lin, J.; Peng, Z.; Huang, K.; Yan, Z.; Cook, N. P.; Samuel, E. L.; Hwang, C.-C.; Ruan, G. Coal as an Abundant Source of Graphene Quantum Dots. *Nat. Commun.* **2013,** *4,*1-6.
6. Yang, F.; Zhao, M.; Zheng, B.; Xiao, D.; Wu, L.; Guo, Y. Influence of Ph on the Fluorescence Properties of Graphene Quantum Dots Using Ozonation Pre-Oxide Hydrothermal Synthesis. *J. Mater. Chem.* **2012,** *22*, 25471-25479.

7. Liu, Y.; Liu, Y.; Park, S.-J.; Zhang, Y.; Kim, T.; Chae, S.; Park, M.; Kim, H.-Y. One-Step Synthesis of Robust Nitrogen-Doped Carbon Dots: Acid-Evoked Fluorescence Enhancement and Their Application in Fe 3+ Detection. *Journal of Materials Chemistry A* **2015,** *3*, 17747-17754.
8. Zhang, X.; Song, G.-J.; Cao, X.-J.; Liu, J.-T.; Chen, M.-Y.; Cao, X.-Q.; Zhao, B.-X. A New Fluorescent Ph Probe for Acidic Conditions. *RSC Adv.* **2015,** *5*, 89827-89832.
9. Staehelin, J.; Hoigne, J. Decomposition of Ozone in Water: Rate of Initiation by Hydroxide Ions and Hydrogen Peroxide. *Environ. Sci. Technol.* **1982,** *16*, 676-681.
10. Yang, F.; Zhao, M.; Wang, Z.; Ji, H.; Zheng, B.; Xiao, D.; Wu, L.; Guo, Y. The Role of Ozone in the Ozonation Process of Graphene Oxide: Oxidation or Decomposition? *RSC Adv.* **2014,** *4*, 58325-58328.
11. Sharma, B. *Instrumental Methods of Chemical Analysis*. 24 ed.; Krishna Prakashan Media: Meerut (UP) India, 2005.
12. Paredes, J.; Villar-Rodil, S.; Solis-Fernandez, P.; Martinez-Alonso, A.; Tascon, J. Atomic Force and Scanning Tunneling Microscopy Imaging of Graphene Nanosheets Derived from Graphite Oxide. *Langmuir* **2009,** *25*, 5957-5968.
13. Chieu, T.; Dresselhaus, M.; Endo, M. Raman Studies of Benzene-Derived Graphite Fibers. *Phys. Rev. B* **1982,** *26*, 1-11.
14. Kikuchi, T.; Sato, S.; Fujita, D.; Fujita, M. Stepwise DNA Condensation by a Histone-Mimic Peptide-Coated M 12 L 24 Spherical Complex. *Chem. Sci* **2014,** *5*, 3257-3260.